Azzouzi, SA.; Vidal Pantaleoni, A.; Bentounes, HA. (2018). Monitoring desertification in Biskra, Algeria using Landsat 8 and Sentinel-1A images. IEEE Access. 6:30844-30854. https://doi.org/10.1109/ACCESS.2018.2837081

Received April 12, 2018, accepted May 11, 2018, date of publication May XX, 2018, date of current version XXX XX, 2018.

Digital Object Identifier

Monitoring desertification in Biskra, Algeria using Landsat 8 and Sentinel-1A images

SOUFIANE ABDELAZIZ AZZOUZI[1,2], ANA VIDAL PANTALEONI[1], (Member, IEEE), AND HADJ ADDA BENTOUNES[2]

[1]Instituto de Telecomunicaciones y Aplicaciones Multimedia (iTEAM), Universitat Politècnica de València, Camino de Vera, València, 46022, Spain
[2]Laboratoire des signaux et systèmes, Faculté des sciences et de la technologie, Université Abdelhamid Ibn Badis de Mostaganem, Mostaganem, 27000, Algeria

Corresponding author: Soufiane Abdelaziz Azzouzi (e-mail: souaz@iteam.upv.es)

ABSTRACT Desertification is the persistent degradation of ecosystems caused by environmental changes and human activities. This is a global problem closely related to climate change with severe consequences in urban locations. For that reason, monitoring those locations with low cost and freely available satellite images could be useful for local agencies. This work studies a strategy for the observation of desertification in Biskra (Algeria) with Landsat 8 images and Synthetic Aperture Radar (SAR) images from Sentinel-1A satellite. Radar images are now available from a growing number of missions. These microwave images add valuable additional information to the existing optical products involving soil roughness and moisture content. They are also a very valuable tool to detect man made objects. However, radar images are still difficult to exploit due to their inherent Speckle noise and their characteristics. This study searches the best methodology for the insertion of radar data to a previously designed approach that uses optical data. Several algorithms are implemented and evaluated and the best technique in terms of overall accuracy and Kappa coefficient is selected for the final change map production. The approach achieves Land Use Land Cover (LULC) change detection using Support Vector Machine (SVM) and segmentation. The most useful change indices are obtained for the best methodology product. The simple improved methodology including radar images provides excellent results and it clearly outperforms the baseline optical technique.

INDEX TERMS Change index, Desertification, Landsat 8, Sentinel-1A, Synthetic Aperture Radar.

I. INTRODUCTION

Desertification is defined by the United Nations Convention to Combat Desertification (UNCCD) in [1] as: “land degradation in arid, semi-arid and dry sub-humid areas resulting from various factors, including climate variation and human activities". The degradation of land cover is a persistent degenerative process that decrease land productivity [2]. This issue is known since last century, but its visibility is growing along with the problem of climate change. So, desertification is a topic of great interest in our days as several studies show especially in China [3], [4] and Africa [5]–[9].

The United Nations Environment Program (UNEP) investigated this subject in [1] and, it promoted in 1994 the United Nations Convention to Combat Desertification (UNCCD). However, the desertification in Africa has become an important problem in the Sahel area [10]. Thus, it is very important to carry out continuous scientific research as explained in [11]. The Algerian Ministry of Agriculture and Rural Development initiated several actions when desertification became a serious threat. Furthermore, the international desertification community also supported those actions that began in the 1960s. The government of Algeria has battled desertification by the following projects [12]:

1) Some vegetal walls were first established in the steppe in order to contain Sahara growth [8]. This program was kept until 1970 using an extensive reforestation policy forming the Green Dam [11]. The width of this vegetation defence was around 20 km and it was located in North of Sahara with the purpose of stopping the advance of the erg (zone with sandy moving dunes in Sahara) [11]. However, the main aim of this project was hardly accomplished, since that barrier is now reduced to a small number of aleppo pines.
2) In the 1970s, a program called the Agrarian Revolution was launched. Its principal goal was to encourage livestock farming in the steppe [8]. Nevertheless, this

project partially failed as a result of complex economic interests that emerged at that time.

3) In 1983, a special institution called 'Haut Commissariat au Développement de la Steppe (HCDS)' was created. Environment preservation and desertification mitigation were the main objectives of this institution. The principal program was focused on pasture recovery and on water well construction. More than 3 million hectares (from 30 million hectares) have been protected in this scheme. On the other hand, this organization has not succeeded in designing a consistent long term policy for the sustainable development of the steppe [8].
4) The project 'Programme National de Développement Agricole (PNDA)' is the most recent initiative against desertification through crop plantation on steppe border grounds.

Desertification is a key topic in global change and some regions like the Sahel have been deeply studied. However, the understanding of this complex issue along with its causes and consequences turns the desertification analysis into a real challenge even now. The problem of desertification in Biskra (Algeria) was studied by the authors in [12] using Landsat 8 data. This city is threatened by desertification since mobile sand dunes are continuously changing due to the wind and orographic conditions. This site has been studied in [13] under a different point of view with focus on soil salinization using decision tree classification. This area was also studied in the modeling of underground dams in [14]. In [9], the desertification from 1987 to 2015 in Biskra was analyzed. Additionally, a study of desertification in Biskra using high and medium resolution satellite data was presented in [15].

This work presents a simple methodology that can be of special interest to local regions that want to monitor their dynamics concerning desertification. There is a broad range of satellite data that allows a systematic analysis in the optical spectrum using passive sensors, and in the microwave spectrum using active sensors like the Synthetic Aperture Radar (SAR). Besides, radar images provide valuable information that is complementary to optical data. Some land features like soil roughness and moisture are clearly best characterized by microwave wavelengths rather than optical ones. SAR images also represent very well man-made objects due to their electrical characteristics. There is a growing number of satellite operators that offer free access to their products. However, the different characteristics of radar and optical data need a careful study in order to select the best approach for the inclusion of radar data into an existing methodology. The authors presented a work on fusion of high resolution optical aerial images and SAR data (X-band) for the detection of houses in [16]. The optimal normalization for optical and SAR images using an Artificial Neural Network (ANN) was presented in [17]. There are also other applications of optical and SAR data fusion: to monitor and study the land cover mapping in [18] and to estimate urban areas and refugee camps in [19], [20]. There is a strong interest in the design of methodologies for the fusion of optical and SAR data tailored to specific applications. However, the problem of desertification has not been studied in the past using SAR and optical data fusion to the authors knowledge. So, the main contribution of this paper is to design the best methodology for change detection using optical and SAR data in the frame of desertification (see section IV-C).

The objective of this work is then to select the best semi-automatic methodology for classification using optical data and C frequency band SAR images (C-SAR) with the final aim of the creation a simple change detection tool that maps sand movement. C-band is a good compromise in the frequency choice 5.40 GHz. Lower frequency (L-band, 1.3 GHz) images might fail in detecting dry sand due to terrain penetration and higher frequency (X-Band, 9.6 GHz) high resolution SAR images were not available at the test site. Support Vector Machine (SVM) has been chosen to classify the area using segmentation. A reduced number of classes has been employed in the legend, since it simplifies the procedure. Biskra (North of Algeria) has been chosen for desertification evaluation because it is a clear point of interest in this topic. Landsat 8 data and Sentinel-1A C-SAR data obtained in 2015 and 2016 were carefully chosen at similar dates.

Different methodologies of classification have been tested in the per object processing chain. Optical data naturally preserve image detail and radar data bring important information about land cover. For that reason, the best methodology for including SAR images, regarding the processing stage in which they are used, has been studied. Speckle filtering has been evaluated in the frame of the proposed procedure. Different polarization channels were also evaluated. Then, the best approach in terms of Overall Accuracy (OA) and Kappa Coefficient (KC) has been selected for further analysis. A number of relevant change detection indices have been chosen to evaluate change using the best methodology. Visually selected pixels have been taken as true data for validation using extra sources of information like high resolution imagery taken at similar dates. These validation regions are obviously different from the training pixels. Finally, the results are fully analyzed taking into account other issues that are also involved in land degradation.

II. STUDY AREA

The zone under analysis is located in the northeastern part of Algeria. It is arid area, limited by the coordinates: (5°32' E, 34°52' N), (5°51' E, 34°52' N), (5°32' E, 34°42' N) and (5°51' E, 34°42' N) as presented in Fig. 1. A subarea with 552.82 km^2 is selected for further analysis. This subarea presents heights above sea level from 87 m to 115 m. The city of Biskra and its surroundings are commonly known as The Door of the Desert. This arid region is surrounded by Occidental Grand Erg (South) and the Mountains of Aurés (North). The population of this city has shown an important increase in 38 years from 95,000 inhabitants in 1977 to

307,987 in 2015. The meteorological data in the zone was given by the Russian Federal Service for Hydrometeorology and Environmental Monitoring. Daily temperatures were very high from June to August. The minimum temperature between 01/01/2015 and 31/12/2016 was 3.0°C, whereas the maximum temperature was 46.0°C. The minimum humidity was 8.0%, and the maximum humidity was 100%. The cumulative annual value of rain was approximately 135 mm. In this

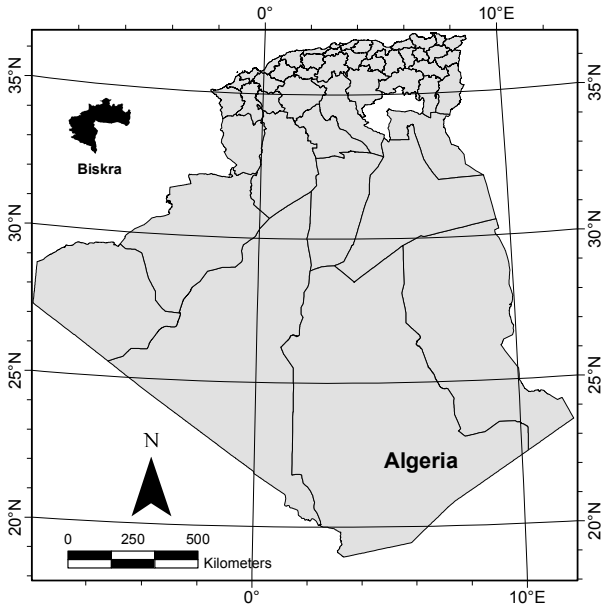

FIGURE 1. Region under study.

region, wind usually blows from southeast towards northwest following Atlas Mountains. The maximum wind velocity in the period of study was 15 m/s as shown in Fig. 2.

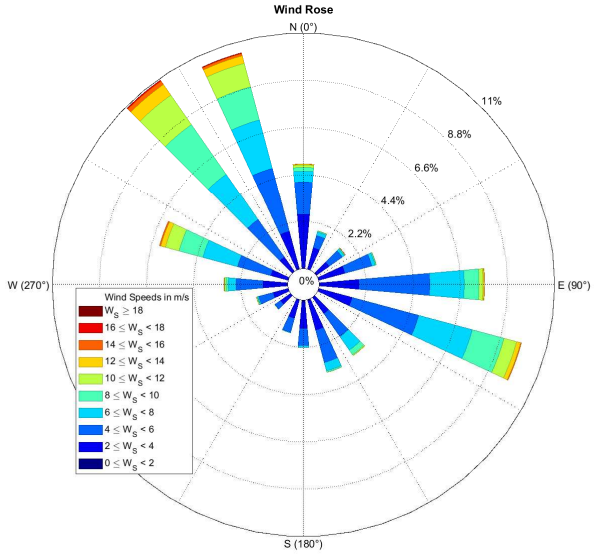

FIGURE 2. Amplitude and direction of the wind from 01/01/2015 until 31/12/2016.

This wind is usually active at the arid season (from June to August), that combined with high temperatures and low moisture cause substantial sand displacement. On the other hand, there are some other issues that may influence sand transportation. One is the presence of vegetation and another is the terrain characteristics concerning topography and soil conditions [12].

III. DATA

The chosen images are taken from the open access archive of the United States Geological Survey (USGS), and from the open access hub Copernicus of the European Space Agency (ESA). Two good quality images of the Landsat 8 program obtained in March are selected (see Table 1). The spectral bands that have been used in this study are the Blue (band 2), Green (band 3), Red (band 4) and Near Infrared (band 5) ones. Two other scenes with processing of level 1 taken by Sentinel-1A satellite (C-SAR) are also selected for the study. The Table 2 shows the characteristics of the radar images. Sentinel-1A contains a dual-polarized radar and two channels are selected for their study: one is the co-polar combination of Vertically polarized incident wave and Vertically polarized backscattered polarization (VV), and the other image contains the cross-polar product Vertically polarized incident Horizontally polarized backscattered wave (VH). The month of March is selected because at that time data form both missions were available at 2015 and 2016 and the optical images presented low cloud content in both scenes. After the definition of the map projection and resolution from the geocorrected images of Landsat 8 and Sentinel-1A, a subarea of 945×650 pixels is selected for the study. This final area presents a pixel spacing of 30×30 m. Landsat 8 images (natural color bands) taken at 2015, 2016 and their corresponding SAR VV images is shown in Fig. 3.

IV. METHODOLOGY

A. OPTICAL DATA PRE-PROCESSING

The energy reflected by the Earth in optical Remote Sensing depends on land cover, which is our objective and some other external factors that must be reduced [21]. The detection of sand movement in a time period is the final goal of this study. So, image correction and co-registration are critical in the overall procedure. For that reason, a pre-processing step including radiometric and geometric corrections is carried out in all images [22]. In this study, radiometric correction based on the Dark Substraction technique is employed (provided by ENVI package). Geometric correction through ground control points is applied as in [23]. Accurate image co-register is also performed using ENVI software with 106 control points [24]. The resulting Root Mean Square Error (RMSE) is equal to 0.32 pixels.

B. RADAR IMAGE PRE-PROCESSING

Radar images are also corrected in this work. The intensity of each pixel represents now the backscattered microwave energy from that area, and that depends on a variety of factors

TABLE 1. Characteristics of the Landsat 8 images.

Acquisition Date	Landsat ID N°	Instrument	Path/ Row	LPGS* version	Data type	Solar azimuth	Solar elevation
16/03/2015	Landsat 8	OLI,TIRS	194/036	2.6.0	L1T	143.75	47.58
02/03/2016	Landsat 8	OLI,TIRS	194/036	2.6.2	L1T	146.38	42.52

* LPGS: Level-1 Product Generation System.

TABLE 2. Characteristics of the Sentinel-1A images.

Acquisition Date	Sentinel Mission	Sensor mode	Product type	Orbit number	Processing level	Polarization
15/03/2015	S1A	IW[1]	GRD[2]	5038	1	DV[3] (dual VV+VH)
08/03/2016	S1A	IW[1]	GRD[2]	10281	1	DV[3] (dual VV+VH)

[1]IW: Interferometric Wide Swath; [2]GRD: Ground Range Detected; [3]DV: Dual polarization.

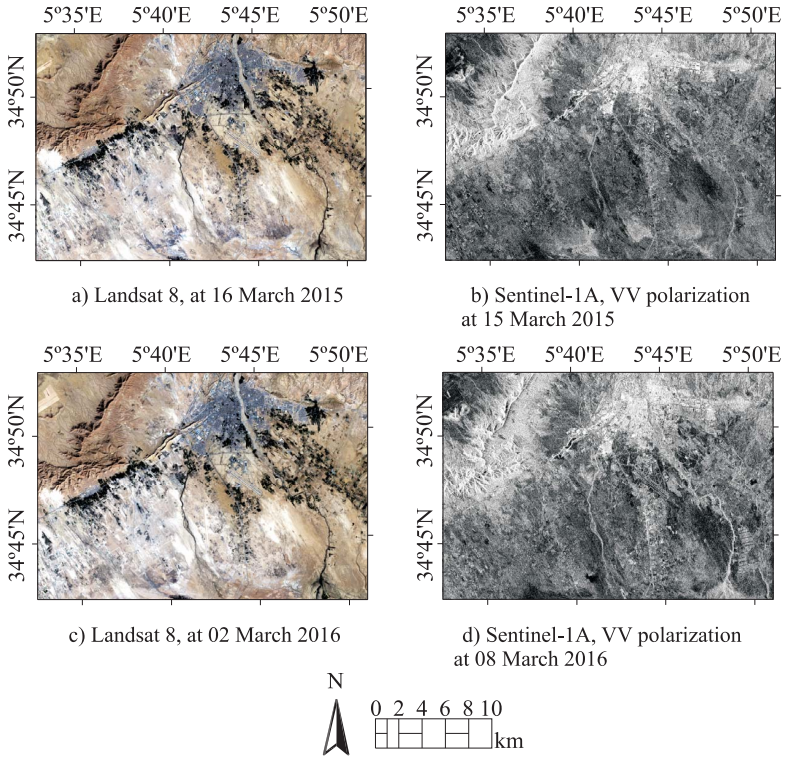

a) Landsat 8, at 16 March 2015

b) Sentinel-1A, VV polarization at 15 March 2015

c) Landsat 8, at 02 March 2016

d) Sentinel-1A, VV polarization at 08 March 2016

FIGURE 3. Landsat 8 images taken at 2015 in a) and 2016 in c), and their corresponding Sentinel-1A images taken at 2015 in b) and 2016 in d).

like soil characteristics and moisture content. The frequency and polarization characteristics of the incident radar pulses and the backscattered echoes are also an important choice. Therefore, radiometric calibration, geometric correction and co-registration are needed to match the optical images in map (WGS84 zone 31 North) and pixel size 30×30 m. SAR images present an inherent noise caused by its relative narrow spectral bandwidth that is called Speckle noise. Speckle noise is caused by constructive and destructive interference of the de-phased coherent return waves scattered by the elementary random scatterers within each resolution cell. This multiplicative noise degrades the interpretation of information, but its reduction can also degrade the texture characteristics in the spatial domain. Speckle noise reduction can be applied either by spatial filtering or multilook processing [25], [26]. A Speckle Lee filter [25] has been selected in this study with the following parameters: 3×3 window size, model with noise mean equal to 1.0, and noise variance equal to 0.25. Figure 4 shows the original VV polarization SAR image obtained in 2015 and its filtered result. In this work, results given by filtered and unfiltered Radar images are properly compared.

C. IMAGE CLASSIFICATION

The Feature Extraction tool of the software ENVI is employed for per object data classification. Attending to this approach, a number of contiguous pixels form an object when they share some properties concerning spatial, spectral or

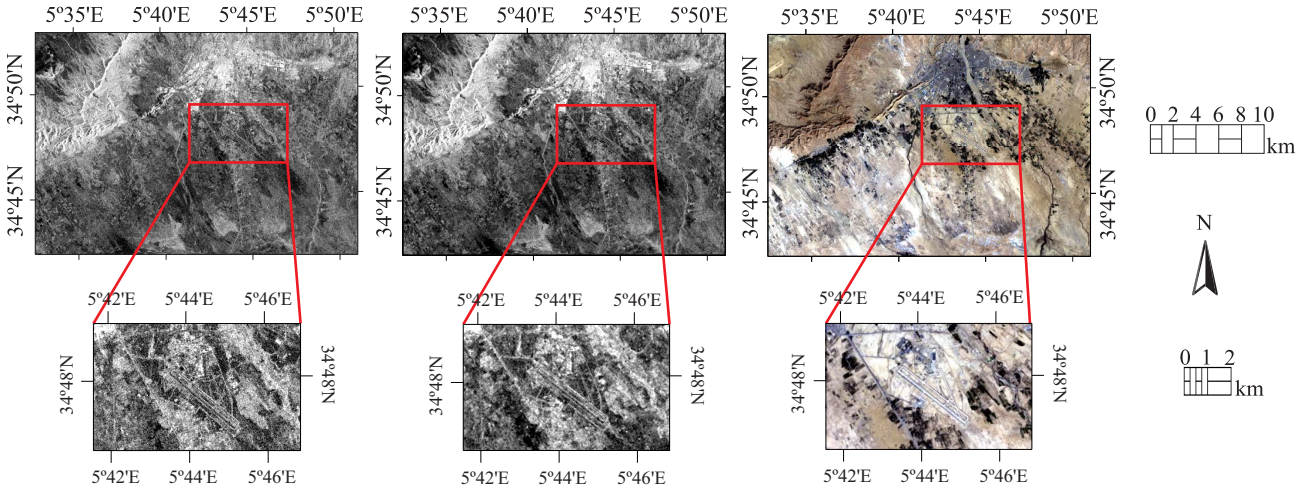

FIGURE 4. SAR and optical images taken at 2015: VV SAR original image in a), Lee filtered VV SAR image in b), and optical image in c).

texture domains. In this work, segmentation uses the edge detection technique with a scale level of 40-45%, a Full Lambda Schedule merging algorithm using a merge value of 60-65%, and a 3×3 pixel texture kernel. These values are obtained after a study in order to get the best result for the different scenes.

The Support Vector Machine (SVM) technique is selected for classification purposes after segmentation. This supervised classification provides the maximum separation between classes. This method was previously used by the authors in [12]. A kernel based on a Gaussian Radial Basis Function (RBF) is chosen for the SVM classifier because it gives the best results after a previous comparative study. The RBF needs the previous choice of two values, the first one is the γ parameter, which changes the kernel width, and the second one is C, which manages the error in the algorithm. As in [12], [27], a previous test is performed in order to get the optimum values for γ (equal to 0.03) and C (equal to 100). The Library for Support Vector Machine designed by [28] and implemented in ENVI is employed in this approach. The training process of the supervised classification is based on the selection of sample regions of pixels of each class. This is a key process carried out by a human operator. By this methodology, 328 training clusters of pixels are chosen for the 2015 images, and 500 clusters of pixels are selected for the 2016 images. In this work, six classes are used for land cover and land use. This few number of classes, shown in Table 3, makes the classification procedure easy for the desertification study.

There are different strategies in order to extract the information from the optical and radar images in the SVM classification process. Some combinations of them are tested and compared in this study. Figure 5 shows the baseline technique for comparison, which is the methodology using optical data presented in [12]. Then some possible techniques that integrate the SAR data are also presented:

TABLE 3. Selected classes used in the study.

Land Cover class	Description
Urban	Buildings, cities, villages, roads
Vegetation	Oases, parklands
Sand	Sands, dunes, erg, and moderately saline regions
Rock	Rock, desert rose, desert mountain
Water	Rivers, lakes, reservoirs
Low dense vegetation (LDV)	Crop fields, grassland

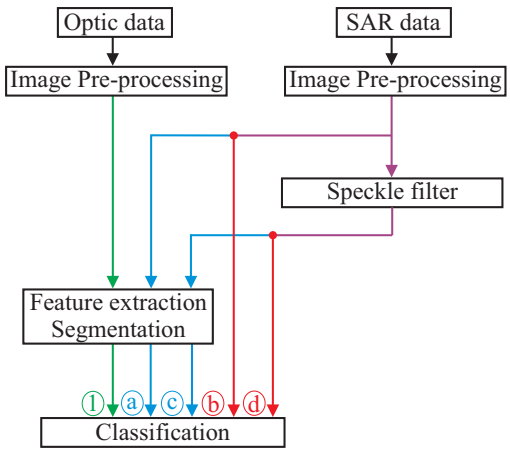

FIGURE 5. Flowchart showing different algorithms for classification of optical data (1), and combining optical and SAR images (a-d).

1) The baseline methodology just uses the Landsat bands for the segmentation and supervised classification. (See Algorithm 1).
2) The second methodology combines optical bands and dual polarization radar images:

a) VV, VH and (VV, VH) polarization SAR images together with the optical data are used in the segmentation process and in the classification. (method (a), see Algorithm 2).
b) VV, VH and (VV, VH) polarization SAR images are not used in the segmentation process, but these images together with the optical data are used to classify. (method (b), see Algorithm 3).
c) A Speckle Lee filter is applied to each radar image for each polarization and then these filtered images are used together with the optical data in the segmentation and the classification processes. (method (c), see Algorithm 2).
d) A Speckle Lee filter is applied to each radar image for each polarization but these filtered images are just used together with the optical data in the classification process. (method (d), see Algorithm 3).

Algorithm 1 Standard classification, method (1)

```
Geometric and radiometric correction
Co-registration
Segmentation and SVM classification
Comparison with truth data
Calculate KC, OA
```

Algorithm 2 SAR and optical fusion including SAR data before segmentation, sf=0 for (a), sf=1 for (c)

```
SAR(1)=VV, SAR(2)=VH, SAR(3)=(VV,VH)
Geometric and radiometric correction
Co-registration
if sf=1 then Apply speckle filter
end if
for i = 1 to 3 do
    Choose the polarization SAR(i)
    Segmentation and SVM classification
    Comparison with truth data
    Calculate KC, OA
end for
```

The objective is to select the best methodology in terms of overall accuracy (OA) and kappa coefficient (KC). These two indices usually describe the accuracy achievement of a confusion matrix. The OA is the ratio of the sum of the diagonal entries to the total number of compared samples N:

$$OA = \frac{\sum_{i=1}^{n} X_{ii}}{N}, \tag{1}$$

where X_{ii} is the diagonal entry of class i and n is the number of classes. The Kappa Coefficient is defined as:

$$KC = \frac{OA - P_e}{1 - P_e}, \tag{2}$$

where P_e is the estimate chance agreement:

$$P_e = \frac{\sum_{i=1}^{n} X_{i+} \cdot X_{+i}}{N^2}, \tag{3}$$

Algorithm 3 SAR and optical fusion including SAR data after segmentation, sf=0 for (b), sf=1 for (d)

```
SAR(1)=VV, SAR(2)=VH, SAR(3)=(VV,VH)
Geometric and radiometric correction
Co-registration
if sf=1 then Apply speckle filter
end if
Segmentation of optical data
for i = 1 to 3 do
    Choose the polarization SAR(i)
    SVM Classification
    Comparison with truth data
    Calculate KC, OA
end for
```

where X_{i+} is the total marginal of row i and X_{+i} is the total marginal of column i.

D. CHANGE DETECTION

Change detection is the spatial identification of change and its type in a time period, according to [29]. This process identifies the change, as well as the previous and posterior classes ("from-to" as in [30]). Therefore, the change detection accuracy relies on image classification [31]. In this work, the evaluation of the change detection is applied to the pair of images acquired at 2015 and 2016. Some change indices are carefully selected for the analysis of land cover change as described in [32] and [12].

V. RESULTS AND DISCUSSION

A. CLASSIFICATION RESULTS

The initial task is to establish the best method to classify the image taking into account the different sources of SAR data (VV, VH or VV+VH polarizations), the stage in which the SAR data is included in the processing chain (before or after segmentation), and the use of a Speckle filter (filtered or not) as proposed in section IV-C. All these possibilities are evaluated using a classification accuracy assessment using visually selected regions for validation purposes. These validation areas are not the same as the training regions used in the supervised classification. For this validation process, 7933 random pixels are visually classified, covering 7.14 km^2 of verified area (1.29% of the entire study zone).

Kappa coefficient and overall accuracy are calculated for each one of the proposed methodology. Table 4 shows the results from this analysis. The worst result is given by the method that uses the Lee filtered VH polarization SAR data for segmentation and classification with 75.94% of overall accuracy in the 2015 set. The best methodology is produced by the method that uses VV polarization without Speckle filtering after the step of segmentation. It produces 97.05% of overall accuracy, 0.96 of Kappa coefficient in 2015, and 96.57% of overall accuracy, 0.96 of Kappa coefficient in 2016. From these results is clear that the best strategy is to consider SAR data only to classify. The segmentation pro-

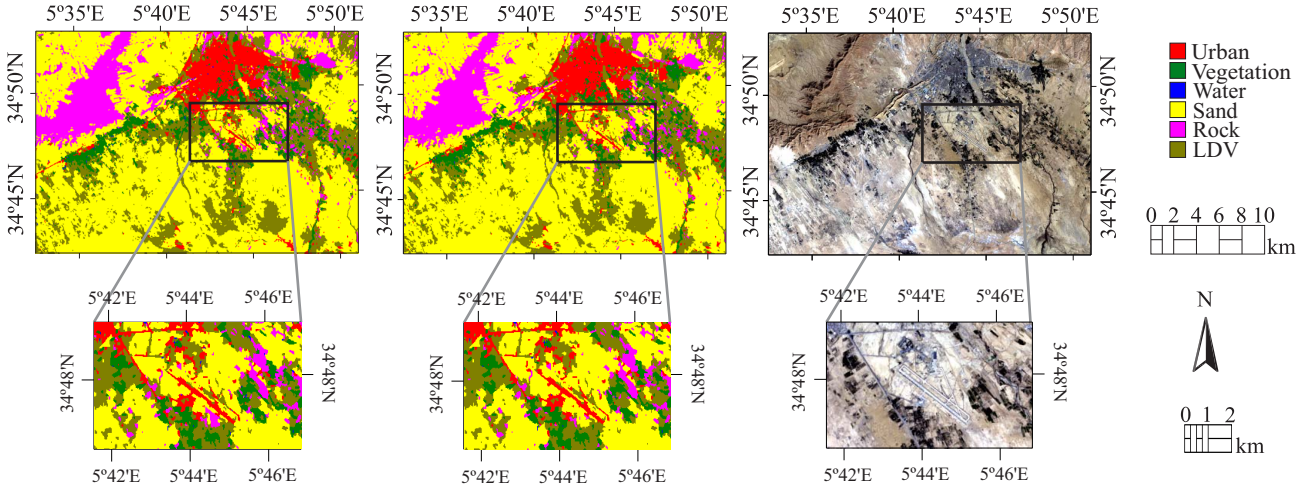

a) Classification result of method (1) b) Classification result of method (b) using VV polarization image c) Optical image

FIGURE 6. Results of the classification in 2015 data with zoom: using method (1) in a), using method (b) and VV polarization in b), optical image in c).

cesses that uses SAR information (in any of its polarization) provide worse results than the techniques that do not use SAR data for segmentation in any case. This should be caused by the poor spatial detail that Radar images give in comparison with optical data of similar spatial resolution. A Speckle filter is also used in order to see any improvement when Speckle noise is reduced. However, Speckle filtering also reduces image texture information, that is useful in the classification stage. In addition, it can be shown that the best results are given by VV polarization channels. VH band does not improve the final result. Then it is clear that the methodology that outperforms the rest is given by the methodology (b) using just VV polarization.

TABLE 4. Classification results given by different methods.

Method of classification	2015		2016	
	OA_1	KC_2	OA_1	KC_2
Optic (1)	86.82	0.83	89.90	0.87
VV before Seg_3(a)	87.28	0.84	90.18	0.88
VV after Seg (b)	**97.05**	**0.96**	**96.57**	**0.96**
VV with Lee filter before Seg (c)	83.18	0.78	86.12	0.83
VV with Lee filter after Seg (d)	84.74	0.80	89.77	0.87
VH before Seg (a)	86.13	0.82	87.38	0.84
VH after Seg (b)	86.90	0.83	89.15	0.86
VH with Lee filter before Seg (c)	75.94	0.69	85.49	0.82
VH with Lee filter after Seg (d)	81.92	0.77	86.75	0.83
DV_4 before Seg (a)	84.74	0.80	88.19	0.85
DV after Seg (b)	87.52	0.84	90.41	0.88
DV with Lee filter before Seg (c)	79.73	0.74	86.02	0.83
DV with Lee filter after Seg (d)	85.32	0.81	87.03	0.84

$_1$OA: Overall accuracy (%); $_2$KC: Kappa coefficient; $_3$Seg: Segmentation; $_4$DV: Dual polarization

A sample of the graphical result obtained for the classification of the 2015 set, using the baseline all optic approach (1) and the best methodology (b) using VV polarization, is shown in Fig. 6.

Tables 5 and 6 show the confusion matrices given by the standard all optic classification in 2015 and 2016, respectively. Tables 7 and 8 show the confusion matrices given by the best methodology including Radar data in 2015 and 2016, respectively. The classification results are much more accurate by using SAR images in the classification process. The overall accuracy successfully increases from 86.82% to 97.05% in the 2015 data set with the selected methodology. It has to be pointed out that the class that gives the poorer results is water, which, on the other hand, is not very frequent in the scene. On the contrary, sand is successfully characterized. The selected best methodology of classification is then used for a deeper desertification analysis in Biskra town.

B. CHANGE DETECTION RESULTS

Once the best classification technique is identified, the evolution of land cover in the study area during one year is evaluated by the observation of the LULC transition matrix [32]. Table 9 shows the transition matrix for the pair of images 2015-2016. The diagonal of the change matrix gives the persistence of each class, and the values not belonging to the diagonal show the type of transition in the classes in that period. The LULC transition table describes that the most important change from 2015 to 2016 was a transition from sand to low dense vegetation, which represents 7.89% of the change. This change is explained by sand migration to the North of Biskra and it is consistent with the usual wind fields. The transition from rock to sand was equal to 2.14% of the change, and the change from urban to sand had a proportion of 0.67%. There is a small amount of vegetation turned into sand (0.10% of the change). Sand class was clearly dominant (54.48%) in the study area in 2016.

A change index is a useful tool to characterize class dynamics in a period of time. They are described in [32] and

TABLE 5. Confusion matrix for the 2015 classification using method (1).

Classes		Ground truth (Pixels)						
		Urban	Vegetation	Water	Sand	Rock	LDV	Commission error
Classified image	Urban	1327	0	0	0	15	4	1.41%
	Vegetation	14	1039	32	0	0	120	13.78%
	Water	2	3	24	0	0	0	17.24%
	Sand	11	0	0	1222	23	10	3.48%
	Rock	97	10	0	78	1860	4	9.22%
	LDV	120	357	4	85	56	1416	30.52%
	Omission error	15.53%	26.26%	60.00%	11.77%	4.81%	8.88%	
Overall accuracy 86.82%, Kappa coefficient 0.83								

TABLE 6. Confusion matrix for the 2016 classification using method (1).

Classes		Ground truth (Pixels)						
		Urban	Vegetation	Water	Sand	Rock	LDV	Commission error
Classified image	Urban	1422	19	3	0	89	7	7.66%
	Vegetation	32	1367	15	0	0	109	10.24%
	Water	0	4	19	0	0	2	24.00%
	Sand	60	0	0	1310	193	7	16.56%
	Rock	36	6	2	47	1672	87	9.62%
	LDV	21	7	28	27	0	1342	5.82%
	Omission error	9.48%	2.57%	71.64%	5.35%	14.43%	13.64%	
Overall accuracy 89.90%, Kappa coefficient 0.87								

TABLE 7. Confusion matrix for the 2015 classification using method (b) using the VV polarization SAR image.

Classes		Ground truth (Pixels)						
		Urban	Vegetation	Water	Sand	Rock	LDV	Commission error
Classified image	Urban	1462	0	0	0	0	4	0.27%
	Vegetation	14	1386	51	0	0	9	5.07%
	Water	0	3	5	0	0	0	37.50%
	Sand	9	0	0	1365	0	10	1.37%
	Rock	2	13	0	0	1954	4	0.96%
	LDV	84	7	4	20	0	1527	7.00%
	Omission error	6.94%	1.63%	91.67%	1.44%	0.00%	1.74%	
Overall accuracy 97.05%, Kappa coefficient 0.96								

TABLE 8. Confusion matrix for the 2016 classification using method (b) using the VV polarization SAR image.

Classes		Ground truth (Pixels)						
		Urban	Vegetation	Water	Sand	Rock	LDV	Commission error
Classified image	Urban	1473	9	3	0	19	3	2.26%
	Vegetation	12	1377	4	0	0	17	2.34%
	Water	0	4	53	0	0	2	10.17%
	Sand	46	0	0	1310	14	0	4.38%
	Rock	9	6	2	47	1921	5	3.47%
	LDV	31	7	5	27	0	1527	4.38%
	Omission error	6.24%	1.85%	20.90%	5.35%	1.69%	1.74%	
Overall accuracy 96.57%, Kappa coefficient 0.96								

TABLE 9. LULC transition matrix (%) from 2015 to 2016.

2015-2016	Urban	Vegetation	Water	Sand	Rock	LDV	Total 2016	Gain
Urban	4.56	0.15	0.01	0.24	0.08	0.59	5.62	1.06
Vegetation	0.11	4.02	0.03	0.09	0.12	0.83	5.20	1.18
Water	0.00	0.00	0.00	0.00	0.00	0.00	0.01	0.01
Sand	0.67	0.10	0.00	46.63	2.14	4.93	54.48	7.85
Rock	0.22	0.09	0.00	1.36	6.69	0.55	8.92	2.22
LDV	1.53	1.51	0.04	7.89	1.29	13.41	25.66	12.25
Total 2015	7.09	5.87	0.09	56.20	10.33	20.31	100	24.58
Loss	2.53	1.85	0.09	9.58	3.63	6.90	24.58	

TABLE 10. LULC change parameters within the landscape in 2015 and 2016 (%).

Classes	Total 2015	Total 2016	Gain	Loss	Persistence	Total Change	Swap	Absolute value of Net Change
Urban	7.09	5.62	1.06	2.53	4.56	3.59	2.12	1.47
Vegetation	5.87	5.20	1.18	1.85	4.02	3.03	2.36	0.67
Water	0.09	0.01	0.01	0.09	0.00	0.10	0.02	0.08
Sand	56.20	54.48	7.85	9.58	46.63	17.43	15.71	1.72
Rock	10.33	8.92	2.22	3.63	6.69	5.86	4.45	1.41
LDV	20.31	25.66	12.25	6.90	13.41	19.15	13.81	5.34
Total	100	100	24.58	24.58	75.31	49	38.47	10.69

they were also used by the authors in [12]. The following indices are selected for this work: Persistence, Gain, Loss, Total change, Swap and absolute value of Net Change. Gain represents the increment of a class use and Loss is the decrement of a class land use in a period of time. Persistence gives an idea of the proportion of a class that does not change and it can be calculated by the difference between the class use at the end of the period and its corresponding Gain. Swap is the class combined Gain and Loss as explained in [32], [33]. The Total Change is the sum of the corresponding class Gain and Loss. The absolute value of Net Change is obtained by the magnitude of the difference between Swap and Total Change as described in [33]. Table 10 shows the presented indices for every class in the time interval from 2015 until 2016. Low dense vegetation class and sand class present high values of Gain (7.85% and 12.25%, respectively) and Loss (9.58% and 6.90%, respectively). That means that these classes are very dynamic in the overall change map. Low dense vegetation and sand also show high values of Swap (15.71% and 13.81%, respectively), according to other class values. This happens because these classes are specially affected by sand movement. Sand dunes are abundant in the erg at the Southwest of Biskra, and they are the main cause of desertification. Water class scarcely changes with a Net Change of 0.08% and a Swap of 0.02% due to its small contribution in the overall scene.

Even in a short time one-year period, there is considerable change in Biskra. Land cover change is remarkable for sand and low dense vegetation classes. The percentage of unchanged area from 2015 until 2016 is 75.31%. Whereas, some kind of change in present in 24.58% of the area.

Some index ratios are also useful in the change detection evaluation. The Loss to Persistence ratio L_p expresses the exposure of a class to change as described in [33]. If L_p is larger than 1, the class is in high risk of changing to other class that will be probably persistent. The L_p value for low dense vegetation is higher than 1 (shown in Table 11) and this implies that this class is inclined to change and to remain in that state. All other classes present values of L_p lower than 1, showing low probability of change.

TABLE 11. Loss to Persistence L_p index, and percentage of change in the period 2015 to 2016.

Land cover	L_p	Percentage of change (%)
Urban	0.55	-1.47
Vegetation	0.46	-0.67
Water	0.00	-0.08
Sand	0.21	-1.72
Rock	0.54	-1.41
LDV	0.51	5.00

The percentage of change shows the potential for overall change of a class as seen in [33]. The Percentage of Change in Table 11 for sand class represents loss of 1.72%, and gain of 5.00% in low dense vegetation, which confirm the transition of sand to low dense vegetation. Therefore, the combination L_p index and the Percentage of Change are relevant tools to control land degradation, which is a key factor in desertification.

Kappa coefficient and overall accuracy are also computed for the change detection product. As in previous validation procedures, the verification data set is different from the training pixels to obtain a rigorous evaluation. Then, 13.45 km^2 (2.43% of the total surface) of ground truth data with 7651 unchanged pixels and 7297 changed pixels are chosen by a human operator. The obtained changed/unchanged confusion matrix using the data obtained in 2015 and 2016 is shown in Table 12 and Table 13. Outstanding results with an overall accuracy equal to 95.29% and a Kappa coefficient of 0.91 are obtained using the classification with inclusion of VV polarization after the segmentation without Lee filter

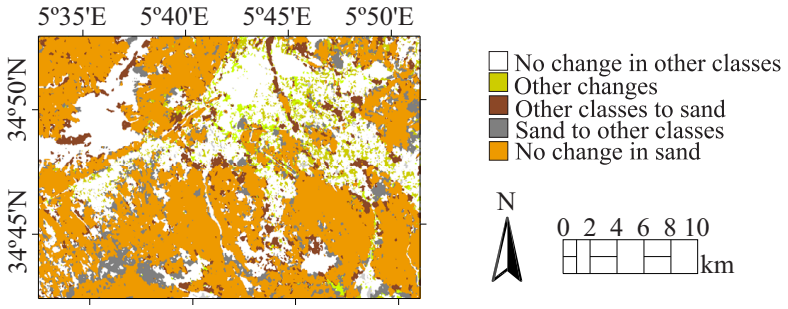

FIGURE 7. Distribution of LULC change between 16/03/2015 and 02/03/2016.

TABLE 12. Change confusion matrix using optical data with the baseline method (1).

Number of pixels		Reference			
		Unchanged pixels	Changed pixels	Sum	Commission error
Classified result	Unchanged pixels	6881	427	7308	5.84%
	Changed pixels	770	6870	7640	10.08%
	Sum	7651	7297	14948	
	Omission error	10.06%	5.85%		
Overall accuracy 91.99%, Kappa coefficient 0.84					

TABLE 13. Change confusion matrix using the best methodology: technique (b) using VV polarization.

Number of pixels		Reference			
		Unchanged pixels	Changed pixels	Sum	Commission error
Classified result	Unchanged pixels	7403	456	7859	5.80%
	Changed pixels	248	6841	7089	3.50%
	Sum	7651	7297	14948	
	Omission error	3.24%	6.25%		
Overall accuracy 95.29%, Kappa coefficient 0.91					

(method (b) using VV polarization). The standard optical classification (method (1)) gives a Kappa coefficient of 0.84 and an overall accuracy equal to 91.99%. These results show the excellent performance of the new classification approach in Biskra using the set of Landsat 8 and Sentinel-1A images.

Fig. 7 shows the spatial distribution of class transitions for the 2015-2016 analysis. Many pixels are changed due to sand displacement with the dominant wind from the Southeast of Sahara. In Biskra, the combination of topography and air flows drives an important sand collection at the Atlas foothills. Fig. 7 shows class change in the time span from 2015 until 2016, where brown color represents change from other classes to sand. The figure shows a very dynamic trend, even in one year of observation, of sand that can indicate a future serious desertification process in the North of Biskra. The transformation from sand to low dense vegetation is mainly caused by human farming activities.

VI. CONCLUSIONS

In this study, the best methodology for including SAR data into an existing algorithm is designed. It has been applied in the evaluation of desertification in the surroundings of Biskra (Algeria) during a period of one year using freely available data from Landsat 8, Sentinel-1A, and local information. Biskra is chosen because it is clearly under risk of desertification due to its proximity to Sahara, its prevalent wind and its topography.

The baseline methodology is based on post-classification change detection using optical data (Landsat) and per-object SVM classification. SAR bands can not be treated in the procedure as extra optical bands due to their different properties. For that reason, a comparative study is presented and some important conclusions are obtained. First, it has been shown that the best approach is to neglect the microwave images for the segmentation process. The inherent noise that is present in the radar images does not help in the object definition step. However, radar image content is used to define the classification rules after segmentation. It has been also shown that a standard Lee Speckle filter does not help in the classification procedure, since it reduces Speckle noise at the cost of removing important texture and detail information. The study finally shows that the use of the cross polarized band does not improve the final result. A simple change detection tool using the Feature Extraction of ENVI software for the fusion of optical and SAR data has been presented. The quality of the analysis has been rigorously evaluated by the corresponding classification and change detection confusion matrices. Besides, very accurate results are achieved with a small set of training data. The selected approach using SAR data clearly outperforms the baseline technique. The most relevant change indices and change maps are then easily produced.

This approach uses open access data and it could be very useful for local and regional authorities. So, future initiatives against desertification could benefit from it.

ACKNOWLEDGMENT

The authors thank the open access hub Copernicus of the European Space Agency (ESA) for the Sentinel-1A images, the United States Geological Survey (USGS) for the Landsat

8 images, and the Met Office of Russian Federal Service for Hydrometeorology and Environmental Monitoring for the provision of the meteorological information.

REFERENCES

[1] U. N. C. on Environment & Development, UNCED (1992) Managing fragile ecosystems: combating desertification and drought. Rio de Janeiro, Brazil: Chapman & Hall, 1992.

[2] A. Grainger, "The role of science in implementing international environmental agreements: The case of desertification," Land Degradation & Development, vol. 20, no. 4, pp. 410–430, 2009.

[3] J. Li, L. Zhao, B. Xu, X. Yang, Y. Jin, T. Gao, H. Yu, F. Zhao, H. Ma, and Z. Qin, "Spatiotemporal variations in grassland desertification based on Landsat images and spectral mixture analysis in Yanchi County of Ningxia, China," IEEE Journal of Selected Topics in Applied Earth Observations and Remote Sensing, vol. 7, no. 11, pp. 4393–4402, 2014.

[4] S. Li and Y. Xie, "Investigating coupled impacts of climate change and socioeconomic transformation on desertification by using multitemporal Landsat images: A case study in central Xilingol, China," IEEE Geoscience and Remote Sensing Letters, vol. 10, no. 5, pp. 1244–1248, 2013.

[5] M. K. Tolba, "Desertification in Africa," Land Use Policy, vol. 3, no. 4, pp. 260–268, 1986.

[6] H. Benmessaoud, F. Chergui, R. Sahnouni, and C. Chafai, "The potential of geomatics in the realization of a map of desertification sensitivity Southern Massif Belezma - Batna - (Algeria)," ISPRS-International Archives of the Photogrammetry, Remote Sensing and Spatial Information Sciences, vol. XL-7/W3, pp. 751–756, 2015.

[7] M. Saifi, N. Boulghobra, and L. Fattoum, "The Green Dam in Algeria as a tool to combat desertification," Planet@Risk, vol. 3, no. 1, pp. 68–71, 2015.

[8] D. Nedjraoui and S. Bédrani, "La désertification dans les steppes algériennes : causes, impacts et actions de lutte," VertigO - la revue électronique en sciences de l'environnement, vol. 8, no. 1, 2008.

[9] M. Mostefaoui, Assessment and analysis of desertification trajectories from 1987 to 2015 in Biskra, the Steppe Region of Algeria. 789 East Eisenhower Parkway, USA: ProQuest, 2017.

[10] A. Aubreville, Climats, forêts, et desertification de l'Afrique Tropicale. France: Société d'Éditions Géographiques, Maritimes et Coloniales, 1949.

[11] A. Marini and M. Talbi, Desertification and risk analysis using high and medium resolution satellite data. Netherlands: Springer Netherlands, 2009.

[12] S. A. Azzouzi, A. Vidal-Pantaleoni, and H. A. Bentounes, "Desertification monitoring in Biskra, Algeria, with Landsat imagery by means of supervised classification and change detection methods," IEEE Access, vol. 5, pp. 9065–9072, 2017.

[13] G. M. Afrasinei, M. T. Melis, C. Buttau, J. M. Bradd, C. Arras, and G. Ghiglieri, "Assessment of remote sensing-based classification methods for change detection of salt-affected areas (Biskra area, Algeria)," Journal of Applied Remote Sensing, vol. 11, pp. 11–28, 2017.

[14] L. Ouerdachi, H. Boutaghane, R. Hafsi, T. B. Tayeb, and F. Bouzahar, "Modeling of underground dams application to planning in the semi arid areas (Biskra, Algeria)," Energy Procedia, vol. 18, pp. 426–437, 2012.

[15] M. Tahar and L. Boureboune, "Anthropic actions and desertification in Algeria," in Desertification and Risk Analysis Using High and Medium Resolution Satellite Data. Dordrecht: Springer Netherlands, 2009, pp. 3–18.

[16] A. Vidal and M. R. Moreno, "Change detection of isolated housing using a new hybrid approach based on object classification with optical and TerraSAR-X data," International Journal of Remote Sensing, vol. 32, no. 24, pp. 9621–9635, 2011.

[17] H. Zhang, H. Lin, and Y. Li, "Impacts of feature normalization on optical and SAR data fusion for land use/land cover classification," IEEE Geoscience and Remote Sensing Letters, vol. 12, no. 5, pp. 1061–1065, May 2015.

[18] J. Neha, B. Matthias, E. Andrea, F. Rasmus, G. Kenneth, H. Patrick, J. M. Rudbeck, K. Tobias, M. Patrick, M. T. A. Edward, R. Johannes, R. M. Casey, and W. Björn, "A review of the application of optical and radar remote sensing data fusion to land use mapping and monitoring," Remote Sensing, vol. 8, no. 1, 2016.

[19] R. Xu, H. Zhang, and H. Lin, "Urban impervious surfaces estimation from optical and SAR imagery: A comprehensive comparison," IEEE Journal of Selected Topics in Applied Earth Observations and Remote Sensing, vol. 10, no. 9, pp. 4010–4021, 2017.

[20] K. Spröhnle, E. M. Fuchs, and P. A. Pelizari, "Object-based analysis and fusion of optical and SAR satellite data for dwelling detection in refugee camps," IEEE Journal of Selected Topics in Applied Earth Observations and Remote Sensing, vol. 10, no. 5, pp. 1780–1791, 2017.

[21] J. Srinivasulu and A. V. Kulkarni, "Estimation of spectral reflectance of snow from IRS-1D LISS-III sensor over the Himalayan terrain," Journal of Earth System Science, vol. 113, no. 1, pp. 117–128, 2004.

[22] W. Y. Yan and A. Shaker, "Radiometric correction and normalization of airborne LiDAR intensity data for improving land-cover classification," IEEE Transactions on Geoscience and Remote Sensing, vol. 52, no. 12, pp. 7658–7673, 2014.

[23] S. Xiangyang, L. Conggui, and S. Yizhen, "Comparison and analysis research on geometric correction of remote sensing images," in 2010 International Conference on Image Analysis and Signal Processing, 2010, pp. 169–175.

[24] R. Reji and R. Vidya, "Comparative analysis in satellite image registration," in 2012 IEEE International Conference on Computational Intelligence and Computing Research, 2012, pp. 1–6.

[25] J. S. Lee and E. Pottier, Polarimetric radar imaging: from basics to applications. CRC Press, Taylor & Francis Group, 2009.

[26] V. S. Frost, J. A. Stiles, K. S. Shanmugan, and J. C. Holtzman, "A model for radar images and its application to adaptive digital filtering of multiplicative noise," IEEE Transactions on Pattern Analysis and Machine Intelligence, vol. PAMI-4, no. 2, pp. 157–166, 1982.

[27] C. Huang, K. Song, S. Kim, J. R. G. Townshend, P. Davis, J. G. Masek, and S. N. Goward, "Use of a dark object concept and support vector machines to automate forest cover change analysis," Remote Sensing of Environment, vol. 112, no. 3, pp. 970–985, 2008.

[28] C. C. Chang and C. J. Lin, "Training V-support vector classifiers: Theory and algorithms," Neural Computation, vol. 13, no. 9, pp. 2119–2147, 2001.

[29] A. G. Yeh and X. Li, "An integrated remote sensing and GIS approach in the monitoring and evaluation of rapid urban growth for sustainable development in the Pearl River Delta, China," International Planning Studies, vol. 2, no. 2, pp. 193–210, 1997.

[30] J. R. Jensen, Introductory digital image processing: a remote sensing perspective, 2nd ed. Prentice Hall, 1995.

[31] D. Yuan and C. Elvidge, "NALC land cover change detection pilot study: Washington D.C. area experiments," Remote Sensing of Environment, vol. 66, no. 2, pp. 166–178, 1998.

[32] R. G. Pontius, E. Shusas, and M. McEachern, "Detecting important categorical land changes while accounting for persistence," Agriculture, Ecosystems & Environment, vol. 101, no. 2, pp. 251–268, 2004.

[33] A. K. Braimoh, "Random and systematic land-cover transitions in northern Ghana," Agriculture, Ecosystems & Environment, vol. 113, no. 1, pp. 254–263, 2006.

SOUFIANE ABDELAZIZ AZZOUZI is currently a PhD student in Telecommunication at Universitat Politècnica de València. He received his Master degree in Industrial Computing from University Abdelhamid Ibn Badis of Mostaganem in 2012. From September 2013 to July 2016, he was an ERASMUS Grant student at Universitat Politècnica de València.

ANA VIDAL-PANTALEONI is an assistant professor at Universitat Politècnica de València. She received the Telecommunication Engineering degree and the PhD degree from the Universitat Politècnica de València. She joined the European Space Agency for two years as a Research Trainee, where her main activity was the study and implementation of software for synthetic aperture radar (SAR) image processing. Her current interests are SAR data processing and Remote Sensing classification for Earth Observation.

HADJ ADDA BENTOUNES , Professor at the University of Mostaganem (Algeria) since 1985, is graduate of the higher school of electricity (Gif/Yvette, Paris), and earned his doctorate in physics of plasmas from the University of Orsay (Paris XI), in 1984. His main subjects of interest are materials physics and environmental systems. He is also president of the Scientific Council of the Mediterranean Foundation of Sustainable Development.